

# Fabrication and Characterisation of Photonic Crystal Slow Light Waveguides and Cavities

## Authors:

Christopher P. Reardon\*, Isabella H. Rey\*, Karl Welna\*, Liam O'Faolain and Thomas F. Krauss

\*C.P.R., I.H.R. and K.W. contributed equally to this work.

## Authors: institution(s)/affiliation(s) for each author:

Christopher P. Reardon  
SUPA School of Physics & Astronomy, University of St Andrews  
St Andrews, Scotland, UK  
Tel: 01334 467336  
Fax: 01334 463104  
[cr39@st-andrews.ac.uk](mailto:cr39@st-andrews.ac.uk)

Isabella H. Rey  
SUPA School of Physics & Astronomy, University of St Andrews  
St Andrews, Scotland, UK  
[ir21@st-andrews.ac.uk](mailto:ir21@st-andrews.ac.uk)

Karl Welna  
SUPA School of Physics & Astronomy, University of St Andrews  
St Andrews, Scotland, UK  
[kw322@st-andrews.ac.uk](mailto:kw322@st-andrews.ac.uk)

Liam O'Faolain (also known as William Whelan-Curtin)  
SUPA School of Physics & Astronomy, University of St Andrews  
St Andrews, Scotland, UK  
[jww1@st-andrews.ac.uk](mailto:jww1@st-andrews.ac.uk)

Thomas F. Krauss  
SUPA School of Physics & Astronomy, University of St Andrews  
St Andrews, Scotland, UK  
[tfk@st-andrews.ac.uk](mailto:tfk@st-andrews.ac.uk)

## Corresponding author:

Christopher P. Reardon

## Keywords:

Photonic Crystals, Slow-light, Cavities, Waveguides, Silicon, SOI, Fabrication, Characterisation

**Short Abstract:** (50 words maximum)

Use of photonic crystal slow light waveguides and cavities has been widely adopted by the photonics community in many differing applications. Therefore fabrication and characterisation of these devices are of great interest. This paper outlines our fabrication technique and two optical characterisation methods, namely: interferometric (waveguides) and resonant scattering (cavities).

**Long Abstract:** (150 words minimum, 400 words maximum)

Slow light has been one of the hot topics in the photonics community in the past decade, generating great interest both from a fundamental point of view and for its considerable potential for practical applications. Slow light photonic crystal waveguides, in particular, have played a major part and have been successfully employed for delaying optical signals<sup>1-4</sup> and the enhancement of both linear<sup>5-7</sup> and nonlinear devices.<sup>8-11</sup>

Photonic crystal cavities achieve similar effects to that of slow light waveguides, but over a reduced band-width. These cavities offer high  $Q$ -factor/volume ratio, for the realisation of optically<sup>12</sup> and electrically<sup>13</sup> pumped ultra-low threshold lasers and the enhancement of nonlinear effects.<sup>14-16</sup> Furthermore, passive filters<sup>17</sup> and modulators<sup>18-19</sup> have been demonstrated, exhibiting ultra-narrow line-width, high free-spectral range and record values of low energy consumption.

To attain these exciting results, a robust repeatable fabrication protocol must be developed. In this paper we take an in-depth look at our fabrication protocol which employs electron-beam lithography for the definition of photonic crystal patterns and uses wet and dry etching techniques. Our optimised fabrication recipe results in photonic crystals that do not suffer from vertical asymmetry and exhibit very good edge-wall roughness. We discuss the results of varying the etching parameters and the detrimental effects that they can have on a device, leading to a diagnostic route that can be taken to identify and eliminate similar issues.

The key to evaluating slow light waveguides is the passive characterisation of transmission and group index spectra. Various methods have been reported, most notably resolving the Fabry-Perot fringes of the transmission spectrum<sup>20-21</sup> and interferometric techniques.<sup>22-25</sup> Here, we describe a direct, broadband measurement technique combining spectral interferometry with Fourier transform analysis.<sup>26</sup> Our method stands out for its simplicity and power, as we can characterise a bare photonic crystal with access waveguides, without need for on-chip interference components, and the setup only consists of a Mach-Zehnder interferometer, with no need for moving parts and delay scans.

When characterising photonic crystal cavities, techniques involving internal sources<sup>21</sup> or external waveguides directly coupled to the cavity<sup>27</sup> impact on the performance of the cavity itself, thereby distorting the measurement. Here, we describe a novel and non-intrusive technique that makes use of a cross-polarised probe beam and is known as *resonant scattering* (RS), where the probe is coupled out-of plane into the cavity through an objective. The technique was first demonstrated by McCutcheon *et al.*<sup>28</sup> and further developed by Galli *et al.*<sup>29</sup>

## **Protocol Text:**

**Disclaimer:** The following protocol gives a general process flow covering the fabrication and characterisation techniques for photonic crystal waveguides and cavities. The process flow is optimised for the specific equipment available in our laboratory, and parameters may differ if other reagents or equipment is used.

### **1.) Sample Preparation**

- 1.1) Sample Cleaving – take the silicon-on-insulator (SOI) wafer and use a diamond scribe to scratch a line approximately 1-2mm long from the edge of the silicon surface, ensuring that the scratch extends over the edge of the wafer. Align the scratch to a straight edge (e.g. that of a microscope slide) and apply even positive pressure to both sides of the scratch: the wafer will cleave along the crystal plane at the scratch location. Repeat this procedure to define the entire chip.
- 1.2) Sample Cleaning –. Place the sample into the CAUTION acetone using tweezers and clean in an ultrasonic bath for 1-2min. Remove the sample from the acetone; rinse any remaining acetone from the sample using CAUTION isopropanol (30s) (both acetone and isopropanol are flammable: use good ventilation and avoid all ignition sources). Dry the sample using a clean dry nitrogen gun.
- 1.3) Spin resist – place the sample onto the spin-coater. Pipette electron sensitive resist CAUTION ZEP520A (ZEP520A is flammable, harmful by inhalation and contact with skin and eyes should be avoided) onto the sample – use enough resist to completely cover the sample without the resist flowing over the edge. Spin the sample so as to give an approx. 350nm thick film and bake on a hotplate at 180°C for 10min. We found this thickness to be the optimal thickness that balances resolution and etch resistance (see later).

### **2.) Pattern Definition**

- 2.1) Design – using appropriate software, simulate the required photonic crystal pattern. A number of useful software packages are available, including but not limited to: MIT Photonic Bands (MPB), FullWAVE™ (RSoft), MIT Electromagnetic Equation Propagation (MEEP).
- 2.2) Pattern Generation – create the exposure files (gds format in general) and proximity error correct using appropriate software.<sup>30</sup>
- 2.3) Pattern Exposure – load the sample into the chamber of the electron beam lithography system (LEO 1530/ Raith Elphy) and pump down. Once vacuum has been achieved, switch on the EHT supply and set to 30kV. Leave the system in this state for 1hr to allow the sample, stage and chamber to reach an equilibrium temperature. Set-up the exposure as indicated in the user-manual of your specific electron beam lithography system. Expose the sample using an appropriate basic step size (e.g. 2nm) (this being the minimum pixel size that the system can expose), a settling time of at least 1ms (this being the time the system waits between moving the beam and exposing the particular portion of the pattern), and an area dose of  $55\mu\text{Acm}^{-2}$ .
- 2.4) Sample Development – using CAUTION Xylene (Xylene is both flammable and highly toxic work in a well-ventilated area away from ignition sources and avoid contact with

skin and eyes) at a temperature of 23°C develop the sample for 45s. Rinse in isopropanol.

### 3.) Patten Transfer

- 3.1) RIE Chamber Cleaning – Set the flow rates of argon and hydrogen to 200sccm. Throttle down the pump, via a butterfly valve, to achieve chamber pressure of  $1 \times 10^{-1}$  mBar. Set the RF power to 100W, ignite the plasma and run for at least 10min – a DC bias of approximately 700V should be observed. After switching off the Ar/H<sub>2</sub> plasma, allow the chamber to pump for approximately 1min. Set the flow rate of oxygen into the chamber to 200sccm and again throttle the chamber pressure down to  $1 \times 10^{-1}$  mBar. Ignite a second plasma of oxygen with a power of 100W and run for 5min. After these procedures, the chamber will be free of contaminants, such as polymer residues, from any previous dry etch. We perform this procedure before every change in etch recipe to ensure maximum repeatability. This procedure is optimised for our system which consists of a parallel-plate, cathode loaded, RIE; with a main chamber 12 inches in diameter by 14 inches in height, including a 12 inch port with both throttling valve and turbo-molecular pump attached.
- 3.2) Photonic Crystal Etching – load the sample into the RIE main chamber and pump the system down to a background pressure of  $<3 \times 10^{-6}$  mBar to ensure the chamber is free of water vapour. Begin the etch by pre-conditioning the chamber with the etching gasses (namely CHF<sub>3</sub> and SF<sub>6</sub>): set the flow rate of both gasses to 100sccm (i.e. set a gas ratio of 1:1) and using the throttle bring the chamber pressure to  $5 \times 10^{-2}$  mBar; allow the gasses to flow for at least 10min. After pre-conditioning, set the RF power to approximately 20W and ignite a plasma; etch the sample for approximately 2min (the etch rate of silicon for these etch parameters is approximately 150nm/min), while ensuring that a chamber pressure of  $5 \times 10^{-2}$  mBar is maintained. A DC bias between 200-220V should be achieved throughout the etching period.
- 3.3) Sample Cleaning to remove remaining electron sensitive resist – after dry etching, clean the sample by rinsing in CAUTION 1165 Remover (1165 is flammable and can cause irritation to eyes, nose and respiratory tract) with ultrasonic agitation for 1-2min, followed by acetone and isopropanol as outlined above (step 1.2).
- 3.4) Membrane Isolation – spin-coat the sample with UV sensitive photo resist CAUTION Microposit S1818 G2 (S1818 G2 is both flammable and causes irritation to eyes, nose and respiratory tract) (see step 1.3). Using an appropriate photomask, define windows within the resist above the photonic crystal patterns using the UV mask aligner. Expose the sample for approximately 30-45s. Develop the resist in CAUTION Microposit Developer MF-319 (MF-319 is an alkaline liquid and can cause irritation to eyes, nose and respiratory tract) for 30-45s, rinsing afterwards in de-ionised water. Prepare a plastic beaker with a mixture of CAUTION 1:5 Hydrofluoric acid (1.1499g/mL 48-51% HF) (HF is extremely corrosive and readily destroys tissue, when handling use full personal protective equipment rated for HF) to de-ionised water. Note that for safety reasons only plastic beakers and tweezers should be used with Hydrofluoric acid. Submerge the sample in the Hydrofluoric acid mixture for 15min. After etching, rinse the sample thoroughly in de-ionised water. Remove the remaining photo-resist using acetone and isopropanol (see step 1.2) – from this stage and onwards ultrasonic agitation cannot be used. To ensure the sample is as clean as possible, follow the acetone and isopropanol wash with a rinse in CAUTION Piranha solution

(Piranha solution is very energetic, potentially explosive and attacks organic materials, when handling use full personal protective equipment) (3:1 CAUTION sulphuric acid (sulphuric acid is corrosive and very toxic, when handling use personal protective equipment and avoid inhalation of vapours or mists) to CAUTION hydrogen peroxide (hydrogen peroxide is very hazardous in case of skin and eye contact, when handling use personal protective equipment)) for 5min, then rinse the sample in de-ionised water, acetone and isopropanol. Note that for safety reasons only glass beakers and metal tweezers should be used with the Piranha solution. As Piranha solution can explode in contact with acetone or isopropanol, it should be handled away from these reagents.

- 3.5) Facet Cleaving – if preparing a photonic crystal slow-light waveguide, the sample requires facet cleaving. Cleave the sample by following the same procedure as outlined in step 1.1, except that as small a scratch as possible should be used. An SOI chip with  $\sim 700\mu\text{m}$  thick substrate can be reliably cleaved down to 4-5mm long samples.

#### 4.) Photonic Crystal Slow-light Waveguide Characterisation

- 4.1) Preliminary preparation of the setup – connect the output of a CAUTION broadband amplified spontaneous emission (ASE) light source (invisible IR radiation: avoid unnecessary high powers, cover beam path if possible) to a 3dB fibre splitter and use each of the outputs to couple light into the two arms of a free-space Mach-Zehnder interferometer (MZI), as shown in Figure 9. Use aspheric lenses to collimate the light output from the fibres. In one of the arms of the interferometer, use two additional aspheric lenses to couple the light beam in and out of the sample chip. Place a polarisation beam splitter (PBS) in the sample arm to TE-polarise the light inputting the sample. Use aspheric lenses to couple the collimated output beams from both arms back into a second 3dB fibre splitter, where they will recombine. Connect one of the outputs to an infrared detector and use the reading of the detector to maximise the light coupling into the sample; connect the other output to an optical spectrum analyser (OSA). The two arms of the MZI should have approximately the same optical length when in the presence of the sample: make sure that the fibres in the two arms of the MZI have the same nominal length and include a tunable delay stage in the reference arm to allow for fine adjustment of its length. In the sample arm, mount the aspheric lenses onto *xyz* precision stages to obtain the best coupling into the sample.
- 4.2) Adjust reference arm length – couple the light beam to a blank (i.e. without photonic crystal) ridge waveguide (of the same type as the access waveguides that feed light inside the photonic crystals) within the same chip in the sample arm. Run a continuous scan on the OSA and observe the measured wavelength spectra. If the two arms of the MZI have approximately the same optical length, the spectra exhibit fringes due to constructive and destructive interference; these fringes will not appear if the arms of the MZI have very different optical lengths ( $>\sim\text{cm}$ ). The fringe spacing is inversely proportional to the difference in optical path length between the two arms. Move the delay stage to make the reference arm shorter and observe the fringes in the OSA: if they become denser (sparser), the reference arm is shorter (longer) than the sample arm. Set the delay stage to make sure that the reference arm is shorter than the sample arm and results in a fringe spacing of about 5 to 10 fringes in a 10nm wavelength range (see Figure 10a). Finally, perform this optimisation on the device that provides the maximum delay and then keep the delay fixed throughout the measurement of the entire sample.

- 4.3) Calibration run – while still aligned on the blank waveguide, run three scans on the OSA: one scan for the interference spectrum and one scan for each of the two arms separately (obtained by blocking the other arm). Use a resolution of 0.05-0.1nm. Record each measured spectrum.
- 4.4) Slow light data acquisition – run and record three spectra as in step 4.3 for each photonic crystal waveguide on the chip.
- 4.5) Fourier data analysis – the interference spectrum (interferogram)  $I(\omega)$  is mathematically expressed by:

$$I(\omega) = S(\omega) + R(\omega) + \text{sqrt}[S(\omega)R(\omega)]\{\exp[i\Phi(\omega) - i\omega\tau] + \text{c.c.}\},$$

where  $S(\omega)$  and  $R(\omega)$  are the spectral densities measured separately from the sample and reference arms, respectively. The delay  $\tau$  is set by the position of the delay stage in the reference arm. The information on the dispersion of the photonic crystal waveguide is contained in the phase term, which we must extract from the measured data.

Subtract the non-interfering background  $S(\omega)+R(\omega)$  from the interferogram to isolate only the interfering term. Calculate the Fourier transform of the interfering term: the term  $\text{sqrt}(SR)\exp[i(\Phi - \omega\tau)]$  and its complex conjugate correspond to peaks centred at  $t=\tau$  and  $t=-\tau$ , respectively. Filter numerically one of the two terms and transform back to the frequency domain. Differentiate the phase  $\Phi(\omega) - \omega\tau$  of the resulting data with respect to  $\omega$  to obtain  $\Delta\tau_g$ , the difference in group delay between the two arms. The group index  $n_g=c/v_g$ , with  $v_g$  the group velocity, is given by:

$$n_g = (\Delta\tau_g^{PhC} - \Delta\tau_g^{cal})c/L + n_{cal},$$

where  $\Delta\tau_g^{cal}$  is obtained from the calibration data taken from the blank waveguide,  $L$  is the photonic crystal waveguide length and  $n_{cal}=2.7$  is the effective index of the reference ridge waveguide. The contribution to the delay from the various optical elements of the setup is taken into account in the calibration run, and is therefore subtracted in this step.

- 4.6) Transmission curve – calculate the transmission curve by normalising the sample spectrum of a photonic crystal waveguide to that of the blank waveguide.

## 5.) Photonic Crystal Cavity Characterisation

- 5.1) Setup – the preparation of the setup (Figure 14) for RS includes: switching of the exchangeable element to the polarising beam splitter; inserting a polariser in the input arm as well as an analyser in the output arm; flip a mirror into the probe arm to allow the use of a near-infrared source; allow the illumination of the sample. Mount the sample vertically with a 45° orientation to axis of the polarizer (Figure 18) on a differential driven  $xyz$  micro-block and adjust the micro-block so that the sample is in focus and a cavity can be seen with the camera, as in Figure 15 (left). Using an amplified spontaneous emission (ASE) source, align the beam with the centre of the cavity Figure 15 (right). Flip away the illumination mirror and allow the output arm to enter the spectrometer (monochromator with attached array detector). Start a broad scan with a low to moderate resolution in order to identify the cavity peaks. Obtain the coarse wavelength of the resonance in the ASE scan (Figure 16a) with an accuracy of

$\pm 1\text{nm}$ . It is also possible to acquire the broad scan with a CAUTION tunable laser source (TLS) (Figure 16b) (invisible IR radiation: avoid unnecessary high powers, cover beam path if possible). One has to be careful that the resolution is set to the highest value in order to sample the line-widths of every peak.

- 5.2) Perform high-resolution scans on the identified peaks – connect the TLS to the input arm and attenuate the beam to a  $\mu\text{W}$  level. Prepare for the high resolution scan by allowing the output arm to be collected by the photodetector and setting up a continuous sweep scan with a resolution of  $1\text{pm}$  for a  $2\text{nm}$  range centred at the previously found resonance wavelength. The importance of this step is to improve the signal-to-noise ratio (SNR) with the aim to obtain a Lorentzian line-shape resonance: change the  $xyz$  position of the micro-block and re-run the scan until the SNR is maximised and the line-shape is close to that of a Lorentzian, as shown in the representative result section.

## Representative Results:

### Fabricated samples:

**Figure 1** shows a scanning electron microscope (SEM) image of an exposed and developed pattern in electron beam resist – it is evident from the “clean” edge between the resist and the silicon substrate that complete exposure/development has been accomplished. Exposure of dose test patterns, consisting of simple repeated shapes (in our case  $50\times 50\mu\text{m}$  squares), each with a differing base dose, are used to determine the correct dose factor and development time for subsequent films.

When creating high resolution features using electron beam lithography, it is beneficial to use as thin a film of resist as possible; when etching the features into silicon, however, it is advisable to use the thickest possible film. Balancing these opposing conditions is the goal of optimising the fabrication recipe: we have found that a layer of ZEP 520A approximately  $350\text{nm}$  thick gives the required high-resolution while still withstanding the etching process.

**Figure 2** shows an SEM image of a second sample which has been exposed, developed and etched using the reactive ion etching (RIE) system: the sample shows vertical sidewalls in each photonic crystal hole and no widening of the holes at either surface of the silicon.

**Figure 3** is of a completed membrane photonic crystal device: the hydrofluoric etch is somewhat isotropic, in that it etches the silica layer nearly equally in every direction. A relatively tight control of the under-etch must therefore be maintained, or too long an etch will cause the photonic crystal membranes to collapse.

In **Figure 4** we present a close-up image of an optimised photonic crystal etch: the vertical sidewalls, the lack of striations and edge-wall roughness are clear to see. This etch was performed using the following parameters: etch pressure  $5 \times 10^{-2}\text{mBar}$ , etch time  $1\text{min } 40\text{s}$ , RF power  $19\text{W}$  producing a DC bias of  $-210\text{V}$ , and  $50:50$  gas ratio of  $\text{SF}_6$  and  $\text{CHF}_3$ .

Increasing the RIE etching pressure above optimum (i.e. to  $5.9 \times 10^{-2}\text{mBar}$ , an increase of  $18\%$ ) introduces an angle in the photonic crystal wall, as can be seen in **Figure 5**. This effect becomes more prevalent as the pressure is increased further. On the other hand, increasing the RF power, which results in a larger DC bias (i.e. RF power of  $22\text{W}$  resulting in a DC bias of  $-232\text{V}$ , increases of  $15\%$  and  $10\%$  respectively), causes a faster break-down of the etch

mask producing a widening of the top of the photonic crystal holes, as can be seen in **Figure 6**. **Figure 7** shows the result of over-etching a photonic crystal, the longer etch time (i.e. 2min 20s, 40% increment) allowing the resist to completely break down resulting in the widening of the photonic crystal holes – creating both of the above effects i.e. photonic crystal hole widening and angled sidewalls. Finally, in **Figure 8** we see the results of poor optimisation of both etch pressure and time: this micrograph indicates that the etch mask has started to break-down causing striations in the photonic crystal holes.

Each of these effects, if not corrected, manifests itself as a higher propagation loss in the final device: propagation losses may arise from both a high density of scattering centres (especially observed in devices with high side-wall roughness) and from a break in symmetry of the photonic crystal structure (as seen in non-verticality and hole widening).<sup>31-32</sup>

### **Measured slow light group index curves:**

A typical example interferogram measured from a blank waveguide is shown in **Figure 10a**. The raw measured data is shown in grey, and is affected by strong Fabry-Perot fringes that result from the high reflectivity at the facets of the waveguide. For clarity, we have numerically filtered out the Fabry-Perot fringes, as shown in the black curve. The fringes resulting from the interference of the sample and reference arms of the MZI setup are clearly visible, and they are uniformly distributed over the entire wavelength range.

The interferogram from an 80 $\mu$ m long engineered slow light photonic crystal waveguide on the same chip is shown in **Figure 10b**: the fringes become denser at wavelengths higher than 1575nm, marking the transition from the fast to the slow light regime. Note that an increase of the group index, corresponding to an increase of the sample arm optical length, will always result in a monotonic reduction of the fringe spacing, as we have deliberately set the delay stage to make sure the reference arm is the shortest.

The corresponding group index curve is shown in **Figure 11** (blue curve): from a value of around 5 in the fast light regime, it increases to around 46, where it remains constant over a bandwidth of ~6nm. The group index curve shown here has been smoothed from the Fabry-Perot noise by performing a running average on the phase term just before differentiation. Note from **Figure 10b** that past the cutoff, where the photonic crystal does not transmit light, there are no fringes, and therefore any resulting group index data at these wavelengths is a measurement artefact.

The transmission curve calculated as the ratio between the transmission of the photonic crystal waveguide and the blank waveguide is also shown as the black line in **Figure 11**, with a sharp cutoff clearly visible around 1594nm.

**Figures 12 and 13** illustrate the capability of our measuring technique: **Figure 12** shows measured group indices in excess of 100 for an 80 $\mu$ m long waveguide, and **Figure 13** shows a measured group index of almost 90 for a 300 $\mu$ m long waveguide. These waveguides were fabricated on the same chip as the waveguides of **Figures 10-11**. The pronounced dips appearing in the transmission curve when approaching the mode cutoff are believed to be the signature of multiple scattering.<sup>33</sup>

### Cavities:

In order to obtain the resonant wavelength and the  $Q$ -factor, the line-shape from the high-resolution scan needs to be fitted. As the coupling to the cavity is governed by Fano resonances, we use the following Fano-function to obtain a proper fit of the line-shape:<sup>14</sup>

$$Y = y_0 + A * ((q + 2 * (\lambda - \lambda_0) / \Delta\lambda)^2 / (1 + (2 * (\lambda - \lambda_0) / \Delta\lambda)^2)),$$

where  $y_0$  is an offset,  $A$  an area constant,  $q$  a dimensionless parameter that gives the ratio between the resonant and non-resonant amplitudes,  $\lambda_0$  is the resonant wavelength and  $\Delta\lambda$  is the full-width half-maximum (FWHM) of the resonance.

In general, the fitting is easier the closer the line-shape is to that of a Lorentzian because, in the first fitting steps,  $q$  can be fixed at 0 and  $\lambda_0$  to the centre of the peak. An example of such a Lorentzian line-shape with a high SNR is shown in **Figure 17a**. The wavelength is determined as 1562.162nm and  $q$  is -0.0891. The  $Q$ -factor is calculated according to:

$$Q = \lambda_0 / \Delta\lambda,$$

so that  $Q$  results in 41,382. In the case that no Lorentzian line-shape can be obtained during the measurement steps in 5.2, the fit is still possible but more difficult, due to more unknown fitting parameters. For example, in **Figure 17b** the peak of the line-shape does not correspond to the resonant wavelength, indicated by the dashed line. The  $Q$ -factor, however, is close to that obtained in **Figure 17a**. If the SNR is low, the fitting error obviously increases, and a Lorentzian line-shape (**Figure 17c**) gives a more accurate  $Q$ -factor than an asymmetric Fano line-shape (**Figure 17d**).

### Tables and Figures:

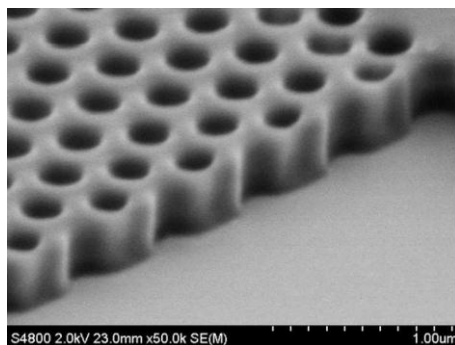


**Figure 1:** Photonic crystal pattern in electron beam resist (ZEP520A).

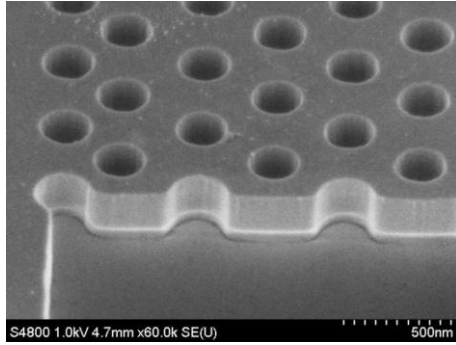


**Figure 2:** Photonic crystal pattern after etching, in silicon.

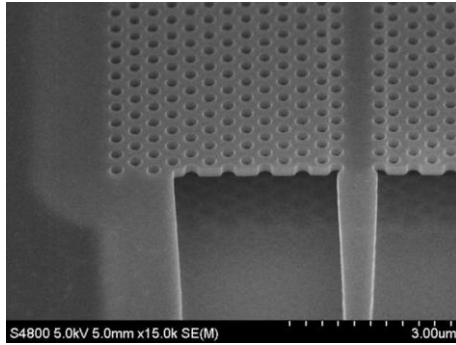


**Figure 3:** Photonic crystal waveguide after undercut etch with hydrofluoric acid.

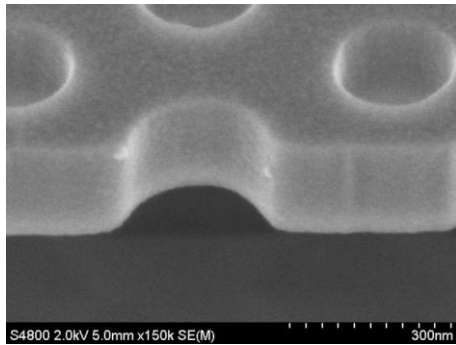


**Figure 4:** Photonic crystal in silicon etched with optimised RIE recipe. Of note are the straight vertical side walls and the little to no side-wall roughness.

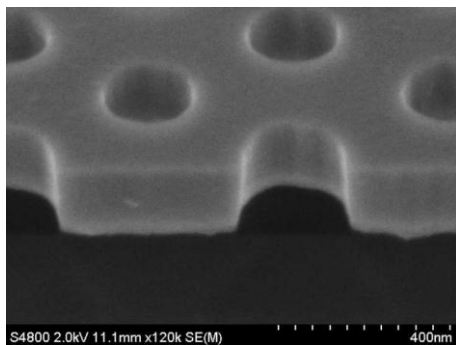


**Figure 5:** Photonic crystal etched with increased RIE chamber pressure. Angled side-walls are evident.

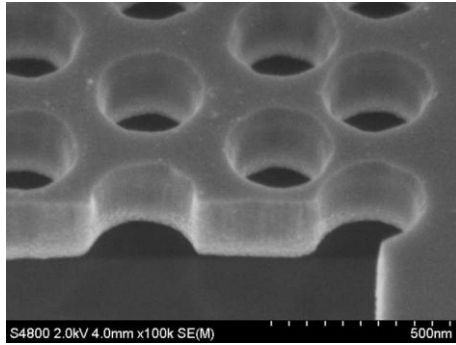


**Figure 6:** Photonic crystal etched with higher RF power (and DC bias). Holes show evidence of widening at surface.

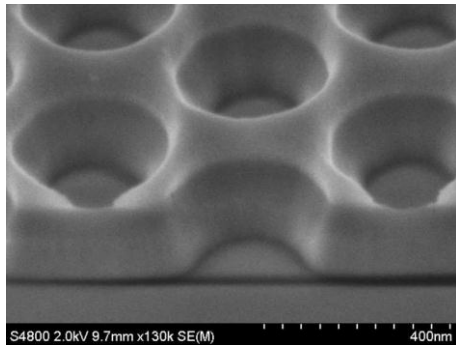


**Figure 7:** Over etched photonic crystal. Angled side-walls due to resist breakdown and overall widening of holes evident.

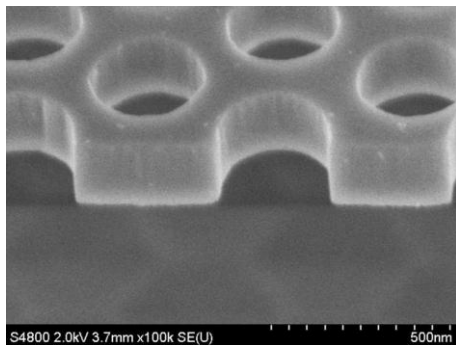


**Figure 8:** Poorly optimised etch (i.e. both pressure and time). Mask break-down has caused striations at the top of each hole.

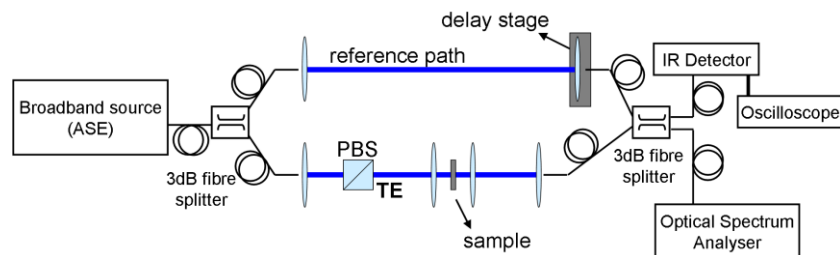


**Figure 9:** Schematic of the Mach-Zehnder interferometric setup used to measure transmission and group index curves of slow light photonic crystal waveguides.

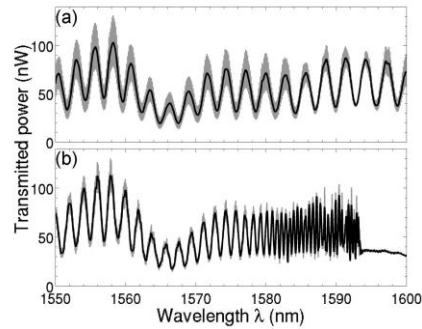


**Figure 10:** Measured interferograms of (a) a blank ridge waveguide and (b) an 80 $\mu\text{m}$  long engineered slow light photonic crystal waveguide on the same chip. The original data is shown as the grey curve in the background. The black curve has been numerically filtered to remove Fabry-Perot fringes.

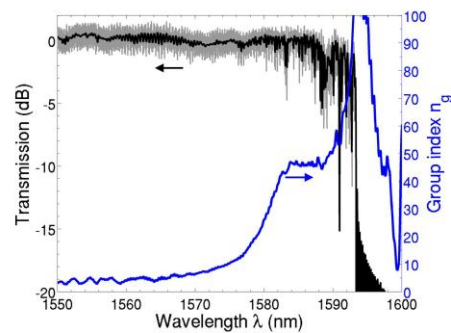


**Figure 11:** Group index (blue) and transmission (black, grey) curves of the same waveguide as in Figure 10(b). The transmission curve is obtained by normalising to that of the blank ridge waveguide. The black curve has been numerically filtered to remove Fabry-Perot fringes.

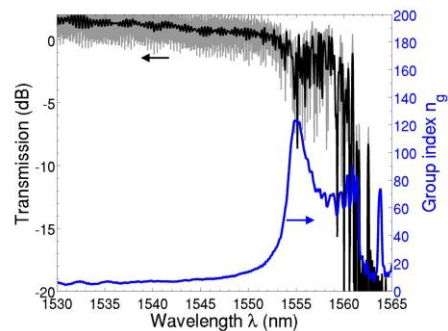


**Figure 12:** Group index (blue) and transmission (black, grey) curves of an 80 $\mu\text{m}$  long waveguide. The transmission curve is obtained by normalising to that of a blank ridge waveguide on the same chip. The black curve has been numerically filtered to remove Fabry-Perot fringes.

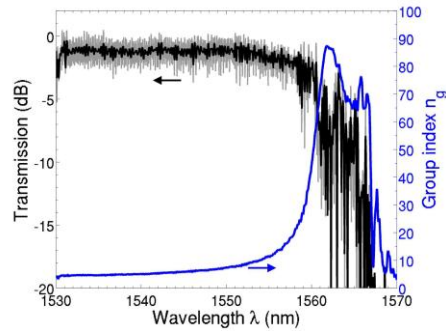


**Figure 13:** Group index (blue) and transmission (black, grey) curves of a 300 $\mu$ m long waveguide. The transmission curve is obtained by normalising to that of a blank ridge waveguide on the same chip. The black curve has been numerically filtered to remove Fabry-Perot fringes.

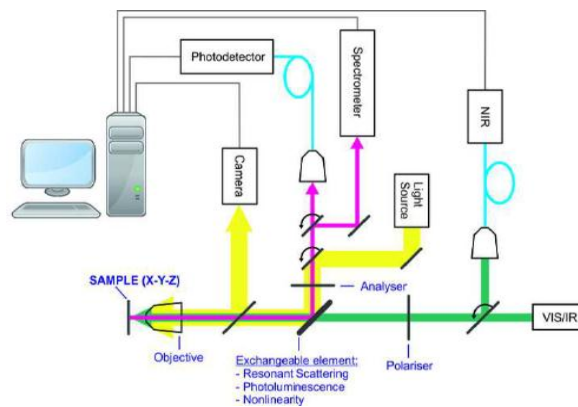


**Figure 14:** Top-view of multi-functional characterisation setup with exchangeable element. The probe beam from the input arm (green) is centred at the high NA objective that focuses it on the mounted sample. Alignment to the centre is obtained by illuminating the cavity with a light source (yellow) and visualising the cavity with the camera. The signal from the output arm (red) can then be directed to a free-space spectrometer or a fibre coupled detector.

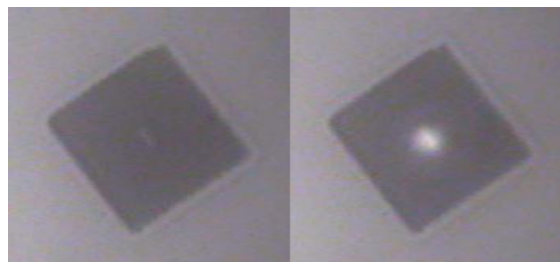


**Figure 15:** Captured image as appears on screen with beam off (left) and on (right). The beam is clearly aligned with the centre of the cavity.

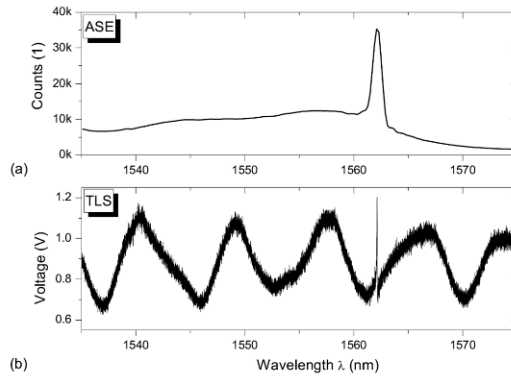


**Figure 16:** Initial broadband scan to identify the cavity resonances. In both the ASE (a) and the TLS (b) scans a strong resonance is visible above 1560nm.

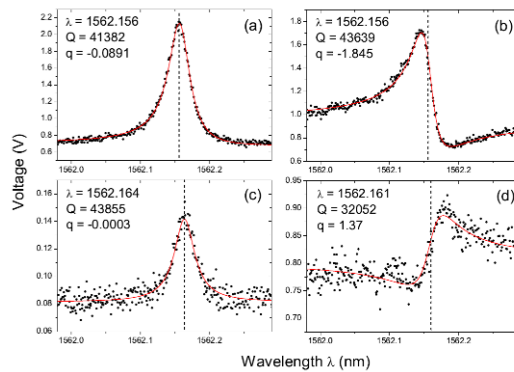


**Figure 17:** High-resolution scans with the TLS. (a) Lorentzian line-shape high SNR. (b) Near Lorentzian line-shape with high SNR. (c) Lorentzian line-shape with low SNR. (d) Asymmetric Fano line-shape with low SNR. The dashed lines indicate the resonance wavelength.

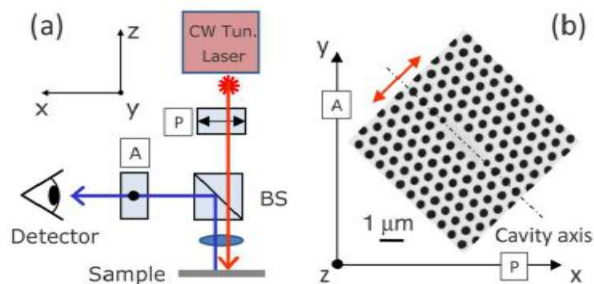


**Figure 18:** Arrangement of polarising optics (a) to the sample (b) (from Reference [29]). The polariser orientates the polarisation in  $x$ -direction and the beam splitter only reflects  $y$ -polarised light, with the analyser further increasing the SNR of  $y$ - to  $x$ -polarised light at the output arm. “Reprinted with permission from Appl. Phys. Lett. 94, 071101. Copyright 2009, American Institute of Physics”

## **Discussion:**

### **Sample fabrication:**

Our choice of electron-beam resist (i.e. ZEP 520A) is due to its simultaneously high resolution and etch resistance. Finally, we believe that ZEP 520A may be affected by the UV light emitted from overhead laboratory lights; as such we recommend placing spin-coated samples in UV opaque containers while moving them from one laboratory to another.

Moving onto defining the photonic crystal pattern, before exposing the sample we have found that allowing the electron beam lithography system to settle for at least an hour after loading reduces mis-alignment errors during writing – this is due to the sample stage and vacuum chamber not being at the same temperature immediately after loading. As photonic crystal patterns, along with access waveguides, may take several hours to write, a small drift in the stage relative to the chamber (even at only nanometres per photonic crystal hole) results in significant stitching and possibly pattern distortion errors with respect to photonic crystal tolerances. This error is random in nature, from one exposure to another, but can be as high as 100 nm/min (absolute positional error), however relative positional error i.e. between one photonic crystal hole to another can be on the order of nanometres, which can be further reduced by increasing the speed at which the pattern is written. As mentioned these issues can be further negated (although never completely removed) by allowing the system to settle after first loading the sample.

The Ar/H<sub>2</sub> plasma etch (used to remove metal and silicon contaminants through ion bombardment) followed by O<sub>2</sub> plasma etch (used for the removal of polymer and organic residue through plasma ashing) described in section 3.1 of the protocol define a cleaning regimen that was developed to control contamination within the RIE chamber when etching the photonic crystals – this cleaning is considered, by us to be one of the most important steps in the fabrication of photonic crystal devices, cleaning of the RIE chamber is paramount to repeatable reliable fabrication especially as in our case where the RIE is not used solely for the etching of silicon. The Ar/H<sub>2</sub> plasma is seen to change from a blue-grey colour (indicating a contaminated chamber) to a pink colour (indicating that the chamber is free of contaminants); a 10min plasma is normally sufficient. The O<sub>2</sub> plasma is then carried out for a further 5-10min depending on the cleanliness of the chamber at the beginning of the process (i.e. Ar/H<sub>2</sub> plasma colour). Although the previous method has not been conclusively proven we find that the colour of the plasma proves a useful indicator for chamber cleanliness. We have also found that by pre-conditioning the etch chamber with the silicon etch gasses for 10min results in a more reliable process – we believe this to be due to the etching gas flow rates stabilising and being adsorbed into the chamber walls during the pre-condition period.

When under-etching the sample, to create membranes, using hydrofluoric acid, the access waveguides must be protected. If the hydrofluoric acid comes into contact with the access waveguide, it penetrates through the now etched trench (either side of the waveguide) and under-etches the access waveguides for hundreds of micrometres. In extreme cases the access waveguides may bend and break due to stresses, rendering a complete chip useless. As hydrofluoric acid is an isotropic etchant, the etching time must be controlled to prevent lateral etching (perpendicular to the photonic crystal waveguide) from causing the membrane to bend due to release of the stress intrinsic to the silicon layer. In extreme cases, the excessive under-etch can also cause the membrane to collapse.

Finally, the creation of clean facets for the free-space coupling of light into photonic crystal waveguides is extremely challenging. If scratched/cleaved carefully, silicon will essentially follow a crystal plane forming a good facet (in our experience, techniques such as facet polishing are not required). A bad facet can cause large coupling losses at each facet. We recommend perfecting a cleaving technique before attempting to work with important samples. It is equally imperative that once a good cleave has been achieved the facets are not damaged: the sample should only be lifted using the two edges parallel to the waveguides (i.e. not by the end facet sides of the chip). Sample lengths down to 2-3mm can be reliably achieved with manual cleaving of a  $\sim 700\mu\text{m}$  thick SOI chip. For smaller samples, we suggest thinning the substrate or use a different cleaving technique.

Although the protocol outlined in this paper is optimised for SOI, the general principle behind the fabrication methods are also valid for the fabrication of devices into other semiconductors, of course when changing from silicon careful consideration of etch-tool, etch-chemistries and mask materials would need to be made.

The fabrication protocol of this paper is optimised for devices targeted at an operating centre wavelength of 1550nm, however devices have also been prepared for the MidIR (2.7-3.5 $\mu\text{m}$ ) regime using fabrication protocols based on the ones presented in this paper.

### **Slow light group index measurements:**

The significance of the group index as the key parameter to measure slow light originates from the dispersion diagram or band structure  $\omega(k)$  typically used to describe the dispersion of a photonic crystal waveguide.<sup>34</sup> The local slope of the dispersion curve  $\partial\omega/\partial k$  corresponds to the group velocity  $v_g$ , i.e. the speed at which the electromagnetic energy travels through the waveguide, which can be equivalently described by the group index  $n_g=c/v_g$ . Values of  $n_g$  around 5 correspond to the fast light regime, whereas higher values are typically considered to fall within in the slow light regime.

When building the slow light MZI setup, it is important to make sure that all the fibres of the two arms of the interferometer are securely tied to the optical table, as any movement or vibration will change the path lengths compromising the quality of the interferogram acquisition. For the same reason, the scan of the interferogram should be performed quickly, or fluctuations of the phase will result in unwanted oscillations of the group index data. The two arms of the MZI may also be realised entirely in free space to avoid fibres altogether, as in Reference [26]: a free-space MZI will be more stable, but also more difficult to align.

Depending on the resolution set and the strength of the Fabry-Perot fringes, the determination of the group index is affected by large uncertainty when the fringes converge very tightly. Setting the delay stage to initially give 4-10fringes/10nm, as detailed in step 4.2 of the protocol, works well for photonic crystal waveguides of lengths 30-100 $\mu\text{m}$  with relatively high group indices, up to  $n_g>100$  for engineered slow light waveguides<sup>35</sup> (see **Figure 12**). For band-edge slow light, the maximum measurable group indices tend to be lower for the same length, due to the higher propagation losses.

With a fringe spacing of  $\sim 4\text{fringes}/10\text{nm}$  we are able to reliably measure group indices up to almost 100 also in 300 $\mu\text{m}$  long engineered waveguides (**Figure 13**). For longer waveguides, the fringes become very dense very quickly, and the resolution of the OSA will limit the maximum measurable group index. Note, however, that for a fixed resolution and fringe

spacing, the maximum measurable group index does not scale linearly with waveguide length, and may also be influenced by propagation loss dispersion. For a very long waveguide, we suggest to include next to it a short waveguide with identical design specifically for group index measurement.

In summary, we have described a simple and powerful method for the experimental determination of the dispersion properties of slow light photonic crystal waveguides. Our technique is based on the combination of frequency domain interferometry<sup>23</sup> with Fourier transform analysis<sup>36</sup> and allows for a direct, single-shot, continuous mapping of the group index curve, with no need for delay scans,<sup>23-24</sup> nonlinear fitting of data<sup>22,25</sup> or determination of the position of fringe extrema.<sup>20-21,25</sup> By using a broadband light source, we are able to extract information from the sample over a large wavelength range, and in a very stable and repeatable manner. We can measure group indices in excess of 100 for both short and moderately long waveguides (up to 200-250 $\mu\text{m}$ ), which are values much higher than those needed for the useful application of slow light waveguides for enhancing the performance of both linear and nonlinear devices.

### **Resonant scattering:**

Photonic crystal cavities confine light in-plane in two dimensions, in contrast to photonic crystal waveguides, where light is guided in one dimension. This allows the storage of light within ultra-small volumes, which is described by an energy decay, analogue to i.e. that of an electronic resonator. In photonic systems, this decay is associated with the photon lifetime of the cavity and is of exponential form, hence resulting in a Lorentzian lineshape of the peak. The ratio of the peak centre wavelength to the Full-Width Half-Maximum represents the  $Q$ -factor.

An important feature of the RS technique is the polarisation maintaining property of the setup and especially that of the high NA objective. Here lies the issue with the compatibility of having a high NA (high collection efficiency) while maintaining the polarisation, because high NA objectives tend to mix polarisations. This polarisation intermixing is responsible for small peaks and low SNR.

When the off-resonance,  $x$ -polarised light arrives at the cavity (**Figure 18a**), it is back scattered through the objective and filtered out by the beam splitter/analyser ( $y$ -polarised), so that only a low level is seen at the detector. In the case of polarisation intermixing, some of the  $x$ -polarised light is converted to the opposite polarisation and can pass the analyser thus increasing the background. If then on-resonance light couples to the cavity, the polarisation rotates for the fundamental cavity mode (red arrow in **Figure 18b**) and creates a  $y$ -polarisation component. This light is directed to the output arm and passes the analyser. Again, the  $y$ -polarised light can convert to the opposite polarisation thus reducing the signal level. Therefore, an objective needs to be chosen so that polarisation intermixing is kept at a minimum.

For ultra-high  $Q$ -factor cavities, such as a hetero-structure cavity, the emitted power is lower. This situation can further reduce the SNR and the peak vanishes in the noise level. A lock-in configuration should then be used to lower the noise level, not the background level, in order to recover the peak.

Note that our setup (**Figure 14**) is designed for multi-functional cavity characterisation, and in addition to RS includes micro-photoluminescence and the generation of second and third harmonic frequencies.

### Acknowledgments:

The authors gratefully acknowledge Dr Matteo Galli, Dr Simone L. Portalupi and Prof. Lucio C. Andreani from the University of Pavia for helpful discussions related to the RS technique and the execution of measurements.

### Disclosures:

The authors have nothing to disclose.

### Reagents:

Name	Company	Catalogue number	Comments (optional)
Acetone	Fisher Scientific	A/0520/17	CAUTION: flammable, use good ventilation and avoid all ignition sources
Isopropanol	Fisher Scientific	P/7500/15	CAUTION: flammable, use good ventilation and avoid all ignition sources
Electron Beam resist	Marubeni Europe plc.	ZEP520A	CAUTION: flammable, harmful by inhalation, avoid contact with skin and eyes
Xylene	Fisher Scientific	X/0100/17	CAUTION: flammable and highly toxic, use good ventilation, avoid all ignition sources, avoid contact with skin and eyes
Microposit S1818 G2	Chestech Ltd.	10277866	CAUTION: flammable and causes irritation to eyes, nose and respiratory tract
Microposit Developer MF-319	Chestech Ltd.	10058721	CAUTION: alkaline liquid and can cause irritation to eyes, nose and respiratory tract
Hydrofluoric Acid	Fisher Scientific	22333-5000	CAUTION: extremely corrosive, readily destroys tissue; handle with full personal protective equipment rated for HF
Microposit 1165 Remover	Chestech Ltd.	10058734	CAUTION: flammable and causes irritation to eyes, nose and respiratory tract
Sulphuric Acid	Fisher Scientific	S/9120/PB17	CAUTION: corrosive and very toxic; handle with personal protective equipment and avoid inhalation of vapours or mists
Hydrogen Peroxide	Fisher Scientific	BPE2633-500	CAUTION: very hazardous in case of skin and eye contact; handle with personal protective equipment

### Equipment:

Name	Company	Catalogue number	Comments (optional)
Silicon-on-Insulator wafer	Soitec	G8P-110-01	
Diamond Scribe	J & M Diamond Tool Inc.	HS-415	
Microscope slides	Fisher Scientific	FB58622	
Beakers	Fisher Scientific	FB33109	
Tweezers	SPI Supplies	PT006-AB	
Ultrasonic Bath	Camlab	1161436	

Spin-Coater	Electronic Micro Systems Ltd.	EMS 4000	
Pipette	Fisher Scientific	FB55343	
E-beam Lithography System	Raith Gmbh	Raith 150	
Reactive Ion Etching System	Proprietary In-house Designed	--	
UV Mask Aligner	Karl Suss	MJB-3	
ASE source	Amonics	ALS-CL-15-B-FA	CAUTION: invisible IR radiation
Single mode fibres	Thorlabs	P1-SMF28E-FC-2	
3dB fibre splitters	Thorlabs	C-WD-AL-50-H-2210-35-FC/FC	
Aspheric lenses	New Focus	5720-C	
XYZ stages	Melles Griot	17AMB003/MD	
Polarising beamsplitter cube	Thorlabs	PBS104	
IR detector	New Focus	2033	
100×Objective	Nikon	BD Plan 100x	
Oscilloscope	Tektronix	TDS1001B	
Optical Spectrum Analyser	Advantest	Q8384	
IR sensor card	Newport	F-IRC2	
TLS source	Agilent	81940A	CAUTION: invisible IR radiation
IR Camera	Electrophysics	7290A	
IR Detector	New Focus	2153	
Digital Multimeter	Agilent	34401A	
Illumination	Stocker Yale	Lite Mite	
Monochromator	Spectral Products	DK480	
Array Detector	Andor	DU490A-1.7	
GIF Fibre	Thorlabs	31L02	

## References:

1. Baba, T., Kawasaki, T., Sasaki, H., Adachi, J. & Mori, D. Large delay-bandwidth product and tuning of slow light pulse in photonic crystal coupled waveguide. *Opt. Express* **16** (12), 9245-9253, doi:10.1364/OE.16.009245 (2008).
2. Melloni, A., Canciamilla, A., *et al.* Tunable delay lines in silicon photonics: coupled resonators and photonic crystals, a comparison. *IEEE Photon. J.* **2** (2), 181-194, doi:10.1109/JPHOT.2010.2044989 (2010).
3. Ishikura, N., Baba, T., Kuramochi, E. & Notomi, M. Large tunable fractional delay of slow light pulse and its application to fast optical correlator. *Opt. Express* **19** (24), 24102-24108, doi:10.1364/OE.19.024102 (2011).
4. Beggs, D. M., Rey, I. H., Kampfrath, T., Rotenberg, N., Kuipers, L. & Krauss, T. F. Ultrafast tunable optical delay line based on indirect photonic transitions. *Phys. Rev. Lett.* **108** (21), 213901, doi:10.1103/PhysRevLett.108.213901 (2012).
5. Beggs, D. M., White, T. P., O'Faolain, L. & Krauss, T. F. Ultracompact and low-power optical switch based on silicon photonic crystals. *Opt. Lett.* **33** (2), 147-149, doi:10.1364/OL.33.000147 (2008).

6. Nguyen, H. C., Sakai, Y., Shinkawa, M., Ishikura, N. & Baba, T. 10Gb/s operation of photonic crystal silicon optical modulators. *Opt. Express* **19** (14), 13000-13007, doi:10.1364/OE.19.013000 (2011).
7. Kampfrath, T., Beggs, D. M., White, T. P., Melloni, A., Krauss, T. F. & Kuipers, L. Ultrafast adiabatic manipulation of slow light in a photonic crystal. *Phys. Rev. A* **81** (4), 043837, doi:10.1103/PhysRevA.81.043837 (2010).
8. Monat, C., Corcoran, B. *et al.* Slow light enhancement of nonlinear effects in silicon engineered photonic crystal waveguides. *Opt. Express* **17** (4), 2944-2953, doi:10.1364/OE.17.002944 (2009).
9. Corcoran, B., Monat, C. *et al.* Green light emission in silicon through slow-light enhanced third-harmonic generation in photonic-crystal waveguides. *Nature Photon.* **3**, 206-210, doi:10.1038/nphoton.2009.28 (2009).
10. Li, J., O'Faolain, L., Rey, I. H. & Krauss, T. F. Four-wave mixing in photonic crystal waveguides: slow light enhancement and limitations. *Opt. Express* **19** (5), 4458-4463, doi:10.1364/OE.19.004458 (2010).
11. Checoury, X., Han, Z. & Boucaud, P. Stimulated Raman scattering in silicon photonic crystal waveguides under continuous excitation. *Phys. Rev. B* **82** (4), 041308, doi:10.1103/PhysRevB.82.041308 (2010).
12. Nomura, M., Kumagai, N., Iwamoto, S., Ota, Y. & Arakawa, Y. Photonic crystal nanocavity laser with a single quantum dot gain. *Opt. Express* **17** (18), 15975-15982, doi:10.1364/OE.17.015975 (2009).
13. Ellis, B., Mayer, M. A. *et al.* Ultralow-threshold electrically pumped quantum-dot photonic-crystal nanocavity laser. *Nature Photon.* **24**, 297-300, doi:10.1038/nphoton.2011.51 (2011).
14. Galli, M., Gerace, D. *et al.* Low-power continuous-wave generation of visible harmonics in silicon photonic crystal nanocavities. *Opt. Express* **18** (25), 26613-26624, doi:10.1364/OE.18.026613 (2010).
15. Notomi, M., Shinya, A., Mitsugi, S., Kira, G., Kuramochi, E. & Tanabe, T. Optical bistable switching action of Si high-Q photonic-crystal nanocavities. *Opt. Express* **13** (7), 2678-2687, doi:10.1364/OPEX.13.002678 (2005).
16. Shambat, G., Rivoire, K., Lu, J., Hatami, F. & Vučković, J. Tunable-wavelength second harmonic generation from GaP photonic crystal cavities coupled to fiber tapers. *Opt. Express* **18** (12), 12176-12184, doi:10.1364/OE.18.012176 (2010).
17. Fan, S., Villeneuve, P. R., Joannopoulos, J. D. & Haus, H. A. Channel drop filters in photonic crystals. *Opt. Express* **3** (1), 4-11, doi:10.1364/OE.3.000004 (1998).
18. Tanabe, T., Nishiguchi, K., Kuramochi, E. & Notomi, M., Low power and fast electro-optic silicon modulator with lateral p-i-n embedded photonic crystal nanocavity. *Opt. Express* **17** (25), 22505-22513, doi:10.1364/OE.17.022505 (2009).
19. Nozaki, K., Tanabe, T. *et al.* Sub-femtojoule all-optical switching using a photonic-crystal nanocavity. *Nature Photon.* **4**, 477-483, doi:10.1038/nphoton.2010.89 (2010).
20. Notomi, M., Yamada, K., Shinya, A., Takahashi, J., Takahashi, C. & Yokohama, I. Extremely large group-velocity dispersion of line-defect waveguides in photonic crystal slabs. *Phys. Rev. Lett.* **87** (25), 253902, doi:10.1103/PhysRevLett.87.253902 (2001).
21. Labilloy, D., Benisty, H., Weisbuch, C., Smith, C. J. M., Krauss, T. F., Houdré, R. & Oesterle, U. Finely resolved transmission spectra and band structure of two-dimensional photonic crystals using emission from InAs quantum dots. *Phys. Rev. B* **59** (3), 1649-1652, doi:10.1103/PhysRevB.59.1649 (1999).

22. Inanç Tarhan, I., Zinkin, M. P. & Watson, G. H. Interferometric technique for the measurement of photonic band structure in colloidal crystals. *Opt. Lett.* **20** (14), 1571-1573, doi:10.1364/OL.20.001571 (1995).
23. Galli, M., Marabelli, F. & Guizzetti, G. Direct measurement of refractive-index dispersion of transparent media by white-light interferometry. *Appl. Opt.* **42** (19), 3910-3914, doi:10.1364/AO.42.003910 (2003).
24. Galli, M., Bajoni, D., Marabelli, F., Andreani, L. C., and Pavesi, L. & Pucker, G. Photonic bands and group-velocity dispersion in Si/SiO<sub>2</sub> photonic crystals from white-light interferometry. *Phys. Rev. B* **69** (11), 115107, doi:10.1103/PhysRevB.69.115107 (2004).
25. Vlasov, Y. A., O'Boyle, M., Hamann, H. F. & McNab, S. J. Active control of slow light on a chip with photonic crystal waveguides. *Nature* **438**, 65-69, doi:10.1038/nature04210 (2005).
26. Gomez-Iglesias, A., O'Brien, D., O'Faolain, L., Miller, A. & Krauss, T. F. Direct measurement of the group index of photonic crystal waveguide via Fourier transform spectral interferometry. *Appl. Phys. Lett.* **90** (26), 261107, doi:10.1063/1.2752761 (2007).
27. Akahane, Y., Asano, T., Song, B.-S. & Noda, S. High-Q photonic nanocavity in a two-dimensional photonic crystal. *Nature* **425**, 944-947, doi:10.1038/nature02063 (2003).
28. McCutcheon, M. W., Rieger, G. W. *et al.* Resonant scattering and second-harmonic spectroscopy of planar photonic crystal microcavities. *Appl. Phys. Lett.* **87** (22), 221110, doi:10.1063/1.2137898 (2005).
29. Galli, M., Portalupi, S. L., Belotti, M., Andreani, L. C., O'Faolain, L. & Krauss, T. F. Light scattering and Fano resonances in high-Q photonic crystal nanocavities. *Appl. Phys. Lett.* **94** (7), 71101, doi:10.1063/1.3080683 (2009).
30. Wüest, R., Strasser, P., Jungo, M., Robin, F., Erni, D. & Jäckel, H. An efficient proximity-effect correction method for electron-beam patterning of photonic-crystal devices. *Microelectron. Eng.* **67-68**, 182-188, doi:10.1016/S0167-9317(03)00070-4 (2003).
31. Tanaka, Y., Asano, T., Akahane, Y., Song, B.-S. & Noda, S. Theoretical investigation of a two-dimensional photonic crystal slab with truncated cone air holes. *Appl. Phys. Lett.* **82** (11), 1661, doi:10.1063/1.1559947 (2003).
32. Asano, T., Song, B.-S. & Noda, S. Analysis of the experimental Q factors (~ 1 million) of photonic crystal nanocavities. *Opt. Express* **14** (5), 1996-2002, doi:10.1364/OE.14.001996 (2006).
33. O'Faolain, L., Schulz, S. A. *et al.* Loss engineered slow light waveguides. *Opt. Express* **18** (26), 27627-27638, doi:10.1364/OE.18.027627 (2010).
34. Joannopoulos, J. D., Johnson, S. G., Winn, J. N. & Meade, R. D. Photonic crystals, molding the flow of light. Princeton University Press, 2nd ed., 2008.
35. Li, J., White, T. P., O'Faolain, L., Gomez-Iglesias, A. & Krauss, T. F. Systematic design of flat band slow light in photonic crystal waveguides. *Opt. Express* **16** (9), 6227-6232, doi:10.1364/OE.16.006227 (2008).
36. Takeda, M., Ina, H. & Kobayashi, S. Fourier-transform method of fringe-pattern analysis for computer-based topography and interferometry. *J. Opt. Soc. Am.* **72** (1), 156-160, doi:10.1364/JOSA.72.000156 (1982).